別紙4
研究成果の刊行に関する一覧表(分子構造イメージングx線回折)
【雑誌】

発表者氏名	論文タイトル名	発表雑誌名	巻号	ページ	出版年
Katanosaka Y, Wakabayashi S, et al	Calineurin Inhibits Na+/Ca2+ Exchange in Phenylephrine-treated Hypertrophic Cardiomyocytes.	J. Biol. Chem	280	5764-5772	2005
Kokubo Y, Inamoto N, Tomoike H, Kamide K, Takiguchi S, Kawano Y, Tanaka C, Katanosaka Y, Wakabayashi S, Shigekawa M, Hishikawa O	Association of Genetic Polymorphisms of Sodium-Calcium Exchanger 1, NCX1, with Hypertension in a Japanese General Population.	Hypertens Res	27; 10	697-702	2004
Woo KJ, Jeong YJ, Inoue H, Park JW, Kwon TK	Chrysin suppresses lipopolysaccharide-induced cyclooxygenase-2 expression through the inhibition of nuclear factor for IL-6 (NF-IL6) DNA-binding	FEBS Lett.	579	705-711	2005
Cherukuri DP, Goulet AC, Inoue H, and Nelson MA	Selenomethionine Regulates cyclooxygenase-2 (COX-2) expression through NF-κB in Colon Cancer Cells.	Cancer Biol Ther	4	175-180	2005
Jing Chen, Min Zhao, Reena Rao, Hiroyasu Inoue, and Chuan-Ming Hao	C/EBP・ and its binding element are required for NF・B induced COX2 expression following hypertonic stress	J. Biol. Chem.	280	16354-16359	2005
Wu CY, Wang CJ, Tseng CC, Chen HP, Wu MS, Lin JT, Inoue H, Chen GH	Helicobacter pylori promote gastric cancer cells invasion through a NF-κB and COX-2-mediated pathway World J Gastroenterol.	J Gastroenterol	11	3197-3203	2005
Yokota C, Kuge Y, Inoue H, Tamaki N, Minematsu K.	Bilateral induction of the S-100A9 gene in response to spreading depression is modulated by the cyclooxygenase-2 activity.	J Neurol Sci.	234	011-016	2005
Park SW, Sung MW, Heo DS, Inoue H, Shim SH, Kim KH.	Nitric oxide upregulates the cyclooxygenase-2 expression through the cAMP-response element in its promoter in several cancer cell lines.	Oncogene	24	6689-6698	2005
Marwaha V, Chen YH, Helms E, Arad S, Inoue H, Bord E, Kishore R, Der Sarkissian R, Gilchrest BA, Goukassian DA.	T-oligo treatment decreases constitutive and UVB-induced COX-2 levels through P53-and NFκB-dependent repression of the COX-2	J Biol Chem.	280	32379-32388	2005
Komatsu K, Buchanan FG, Katkuri S, Morrow JD, Inoue H, Otaka M, Watanabe S, Dubois	Oncologenic potential of MEK1 in rat intestinal epithelial cells Is mediated via cyclooxygenase-2.	Gastroenterology	29	577-590	2005
Lim WC, Park M, Bahn JJ, Inoue H, Lee YJ.	Hypertonic sodium chloride induction of cyclooxygenase-2 occurs independently of NF-κB and is inhibited by the glucocorticoid receptor	FEBS Lett.	579	5430-5436	2005
Okawa T, Naomoto Y, Nobuhisa T, Takaoka M, Motoki T, Shirakawa Y, Yamatsuji T, Inoue H, Ouchida M, Gunduz M,	Heparanase is involved in angiogenesis in esophageal cancer through induction of cyclooxygenase-2. Clin Cancer Res.	Clin Cancer Res.	11	7995-8005	2005
Na HK, Inoue H, Surh YJ.	ET-18-O-CH3-induced apoptosis is causally linked to COX-2 upregulation in H-ras transformed human breast epithelial cells.	FEBS Lett.	579	6279-6287	2005
Sato, E., Germer, R., Tanaka, E., Mori, H., Kawai, T., Ichimaru, T., Sato, S., Ojima, H., Takayama, K., Ido, H	Quasi-monochromatic cerium flash angiography.	SPIE	5580	146-152	2005

Sato, E., Germer, R., Tanaka, E., Mori, H., Kawai, T., Ichimaru, T., Sato, S., Ojima, H., Takayama, K., Ido, H.	Weakly ionized linear plasma x-ray generator with molybdenum-target tride.	SPIE	5580	535-542	2005
Sato, E., Sagae, M., Komatsu, M., Germer, R., Tanaka, E., Mori, H., Kawai, T., Ichimaru, T., Sato, S., Ojima, H., Takayama, K., Ido, H.:	Monochromatic flash x-ray generator utilizing copper-target diode.	SPIE	5580	579-585	2005
Sagae, M., Sato, E., Obara, H., Tanaka, E., Mori, H., Kawai, T., Sato, S., Ojima, H., Takayama, K., Ido, H.	Intense quasi-monochromatic flash x-ray generator utilizing molybdenum-target diode.	SPIE	5580	674-680	2005
Sato, E., Tanaka, E., Mori, H., Kawai, T., Sato, S., Ojima, H., Takayama, K., Ido, H	Energy selective high-speed radiography utilizing stroboscopic x-ray generator.	SPIE	5580	765-771	2005
Sato, E., Sagae, M., Obara, H., Germer, R., Tanaka, E., Mori, H., Kawai, T., Ichimaru, T., Sato, S., Ojima, H., Takayama, K., Ido, H	Demonstration of flash K-edge angiography utilizing gadolinium-based contrast medium.	SPIE	5580	817-823	2005
Obara, H., Sato, E., Tanaka, E., Mori, H., Kawai, T., Ichimaru, T., Sato, S., Ojima, H., Takayama, K.,	Superposition of x-ray spectra using a double-target plasma tube.	SPIE	5580	824-831	2005
Sato, E., Tanaka, E., **Mori, H.**, Kawai, T., Ichimaru, T., Sato, S., Takayama, K., Ido, H.	Compact monochromatic flash x-ray generator utilizing a disk-cathode molybdenum tube.	Med. Phys.	32	49-54	2005
Sagae, M., Sato, E., Tanaka, E., Hayasi, Y., **Mori, H.**, Kawai, T., Ichimaru, T., Sato, S., Takayama, K., Ido, H.	Quasi-monochromatic X-ray generator utilizing graphite cathode diode with transmission-type molybdenum target.	Jpn. J. Appl. Phys.	44	446-449	2005
Hattan, N., Kawaguchi, H., Ando, K., Kuwabara, E., Fujita, J., Murata, M., Suematsu, M., Mori,	Purified cardiomyocytes from bone marrow mesenchymal stem cells produce stable intracardiac grafts in	Cardiovasc. Res.	65	334-344	2005
Yada, T., Shimokawa, H., Hiramatsu, O., Kajita, T., Shigeto, F., Tanaka, E., Shinozaki, Y., **Mori, H.**, Kiyooka, T., Katsura, M., Ohkuma, S., Masami, Goto,	Beneficial effect of hydroxyfasudil, a specific Rho-kinase inhibitor, on ischemia-reperfusion injury in canine coronary microcirculation in vivo.	JACC	45	599-607	2005
Fujii, T., Nagaya, N., Iwase, T., Murakami, S., Miyahara, Y., Nishigami, K., Ishibashi-Ueda, H., Shirai, M., Itoh, T., Ishino, K., Sano, S., Kangawa, K., Mori, H.	Adrenomedullin enhances therapeutic potency of bone marrow transplantation for myocardial infarction in rats.	Am. J. Physiol. Heart. Circ. Physiol.	288	H1444 - H1450	2005
Sato, E., Tanaka, E., Mori, H., Kawai, T., Inoue, T., Ogawa, A., Sato, S., Takayama, K., Ido, H.	High-speed K-edge angiography achieved with tantalum K-series characteristic x rays.	SPIE	5745	810-817	2005
Sato, E., Tanaka, E., Mori, H., Kawai, T., Sato, S., Takayama, K.	High-speed enhanced K-edge angiography utilizing cerium plasma x-	Opt.Eng.	44	049001(1-6)	2005
Sato, E., Tanaka, E., Mori, H., Kawai, T., Sato, S., Takayama, K.	Clean monochromatic x-ray irradiation from weakly ionized linear copper	Opt.Eng.	44	049002(1-6)	2005
Kawada, T., Yamazaki, T., Akiyama, T., Shishido, T., Mori, H., Sugimachi, M.	Myocardial interstitial choline and glutamate leels during acute myocardial ischemia and local ouabain	Acta.Phisiol. Scand.	184	187-193	2005
Hirata, A., Minamino, T., Asanuma, H., Sanada, S., Fujita, M., Tsukamoto, O.	Erythropoietin just before reperfusion reduces lethal arrhythmias and infarct size via phosphatidylinositol-3 kinase-dependent pathway in canine hearts.	Cardiovasc.Drug s.Ther.	19	33-40	2005
Kitagawa, H., Yamazaki, T., Akiyama, T., Sugimachi, M., Sunagawa, K., Mori, H.	Microdialysis separately monitors myocardial interstitial myoglobin during ischemic and reperfusion.	Am.J.Physiol.Heart.Circ.Physiol.	289	H924-H930	2005

Nagaya, N., Kangawa, K., Itoh, T., Iwase, T., Murakami, S., Miyahara, Y., Fujii, T., Uematsu, M., Ohgushi, H., Yamagishi, M., Tokudome, T., Mori, H.,	Transplantation of mesenchymal stem cells improves cardiac function in a rat model of dilated cardiomyopahy.	Circulation	112	1128-1135	2005
Kuroko, Y., Fujii, T., Yamazaki, T., Akiyama, T., Ishino, K., Sano, S., Mori H.	Contribution of catechol O-methyltransferase to the removal of accumulated interstitial catecholamines evoked by myocardial ischemia.	Neuroscience Letters,	388	61-64	2005
Ben Ammar, Y., Takeda, S., Sugawara, M., Miyano, M., Mori, H., Wakabayashi, S.	Crystallization and preliminary crystallographic analysis of the human calcineurin homologous protein CHP2 bound to the cytoplasmic region of the Na+/H+ exchanger NHE1. Acta Cryst.	Acta Cryst	Section F Structural Biology and Crystallization Communications	956-958	2005
Sato, E., Yamadera, A., Ichimaru, T., Tanaka, E., Mori, H., Kawai, T., Inoue, T., Ogawa, A., Sato, S., Takayama, K.	Conventional Enhanced K-edge angiography Utilizing cerium x-ray generator.	原子核研究	49	69-74	2005
Sato, E., Tanaka, E, Mori, H., Kawai, T., Inoue, T., Ogawa, A., Sato, S., Takayama, K., Ido, H.	Preliminary experiment for producing higher harmonic x rays utilizing copper plasma triode.	原子核研究	49	61-67	2005
Ichimaru, T., Sato, E., Tanaka, E., Mori, H., Kawai, T., Sato, S., Takayama, K.	Quasi-monochromatic fine polycapillary imaging utilizing a computed radiography system.	Bull.Health, Sci. Hirosaki,	4	83-91	2005
Ichimaru, T., Yamadera, A., Sato, E., Tanaka, E., Mori, H., Kawai, T., Sato, S., Takayama, K.	Cone-beam K-edge angiography utilizing cerium x-ray tube in conjunction with cerium oxide filter.	Bull.Health, Sci. Hirosaki	4	93-100	2005
Sato, E., Tanaka, E., Mori, H., Kawai, T., Inoue, T., Ogawa, A., Sato, S., Ito, F., Takayama, K., Onagawa, J., Ido, H	Variations in cerium x-ray spectra and enhanced K-edge angiography.	Jpn.J.Appl.Phys.	44	8204-8209	2005
Sato, E., Hayasi, Y., Kimura, K., Tanaka, E., Mori, H., Kawai, T., Inoue, T., Ogawa, A., Sato, S., Takayama, K., Onagawa, J., Ido,	Enhanced K-edge angiography utilizing tantalum plasma x-ray generator in conjunction with gadolinium-based contrast media.	Jpn.J.Appl.Phys	44	8716-8721	2005
Sato, E., Tanaka, E., Mori, H., Kawakami, H., Kawai, T., Inoue, T., Ogawa, A., Sato, S., Ichimaru, T., Takayama, K., Ido, H.	Enhanced magnification angiography including phase-contrast effect using a 100-um focus x-ray tube.	SPIE	5918	591811;1-9	2005
Sato, E., Tanaka, E., Mori, H., Kawai, T., Inoue, T., Ogawa, A., Ichimaru, T., Takayama, K., Ido,	Monochromatic x-ray generator utilizing angle dependence of bremesstrahlung x-ray distribution.	SPIE	5918	591819;1-7	2005
Sato, E., Hayasi, Y., Germer, R., Kimura, K., Tanaka, E., Mori, H., Kawai, T., Inoue, T., Ogawa, A., Sato, S., Takayama, K., Ido H.	Energy-selective gadolinium angiography utilizing a stroboscopic x-ray generator.	SPIE	5920	59200V;1-8	2005
Sato, E., Hayasi, Y., Germer, R., Obara, H., Tanaka, E., Mori, H., Kawai, T., Inoue, T., Ogawa, A., Sato, S., Takayama, K., Ido, H.	Preliminary study for producing higher harmonic hard x-rays from weakly ionized copper plasma.	SPIE	5920	59200U;1-7	2005
Obara, H., Sato, E., Hayasi, Y., Tanaka, E., Mori, H., Kawai, T., Inoue, T., Ogawa, A., Takayama, K., Ido, H.	Superposition of x-ray spectra using a brass-target plasma triodea.	SPIE	5920	59200W;1-8	2005
Sato, E., Hayasi, Y., Germer, R., Kimura, K., Tanaka, E., Mori, H., Kawai, T., Inoue, T., Ogawa, A., Sato, S., Takayama, K., Ido, H.	Enhanced K-edge plasma angiography achieved with tungsten Karays utilizing gadolinium-based contrast media.	SPIE	5920	592012;1-8	2005

Sato, E., Hayashi, Y., Germer, R., Tanaka, E., Mori, H., Kawai, T., Inoue, T., Ogawa, A., Sato, S., Ichimaru, T., Takayama, K., Onagawa, J., Ido, H.	Monochromatic flash x-ray generator utilizing a disk-cathode silver tube.	Opt.Eng.	44	096501(1-6)	2005
Sato, E., Yamadera, A., Tanaka, E., Mori, H., Kawai, T., Ito, F., Inoue, T., Ogawa, A., Sato, S., Takayama, K., Onagawa, J., Ido,	X-ray spectra from cerium target and their application to cone beam K-edge angiography.	Opt.Eng.	44	096502(1-6)	2005
Schwenke, D.O., Pearson, J.T., Tsuchimochi, H., Mori, H., Shirai, M.	Exogenous nitric oxide centrally enhances pulmonary reactivity in the normal and hypertensive rat.	Clinical and experimental pharmacology and physiology	32	952-959	2005
Sato, E., Tanaka, T., Mori, H., Kawai, T., Inoue, T., Ogawa, A., Takahashi, K., Sato, S., Takayama, K.	X-ray spectra from characteristic x-ray generator with a molybdenum tube.	Annual Report of Iwate Medical University, School of Liberal Arts and	40	1-7	2005
Sato, E., Tanaka, E., Mori, H., Kawai, T., Inoue, T., Ogawa, A., Takahashi, K., Sato, S., Takayama, K.	Measurement of cerium x-ray spectra using a cerium oxide powder filter and enhanced K-edge angiography.	Annual Report of Iwate Medical University, School of Liberal Arts and	40	1-7	2005
Takeda, S.	Crystal structure of troponin and the molecular mechanism of muscle regulation.	Journal of Electron Microscopy	52(Suppl.1)	i-35-41	2005
Nagaya, N., Mori, H., Murakami, S., Kangawa, K., Kitamura, S.	Adrenomedullin: angiogenesis and gene therapy. (Invited Reviw)	Am.J.Physiol.Regul.Integr.Comp. Physiol.	288	R1432-R1437	2005
佐藤英一、林 保臣、小原春雄、田中越郎、盛 英三、河合敏昭、井上 敬、小川 彰、佐藤成大、市丸俊夫、高山和喜、臼杵辰巳、佐藤公悦	シンクロトロンにかわる医用単色X線装置の開発と応用.	医学物理	25	25-38	2005
久光隆、若林繁夫	トランスポータ研究のいま—Na+/H+交換輸送体を中心に	化学と生物	44(1)	56-65	2006
井上 裕康	PPARsの内因性リガンド	日本臨床	63	578-583	2005
井上 裕康	「フレンチパラドックス」と核内受容体PPARとの新しい接点	化学と生物	43	619-624	2005
宮原義典、盛英三、永谷憲歳	特集Ⅱ 第68回日本循環器学会学術集会2. 日本型移植医療をどう作るか—細胞・組織・臓器 心血管疾患における細胞一遺伝子ハイブリッド治療.	循環器専門医	13	33-39	2005
増田道隆, 小形尚子, 望月直樹	PECAM-1を介した血管内皮細胞のメカノセンシング.	日薬理誌	124	311－318	2004
盛 英三、望月 直樹、武田 壮一、井上 裕康、中村 俊、土屋 利江	ナノレベルとイメージングによる分子構造と機能の解析	日本臨牀	64巻2号	358-364	2006

別紙４
研究成果の刊行に関する一覧表（ナノ構造解析に基づく医用材料開発）

【雑誌】

発表者氏名	論文タイトル名	発表雑誌名	巻名	ページ	出版年
Nakazawa, Ken Ohno,Yasuo	Charactarization of voltage-dependent gaiting of P2X2 receptor/channel.	European Journal of Pharmacology	508	23-30	2005
Nakazawa, Ken Yamakoshi, Yoko Tsuchiya, Toshie Ohno,Yasuo	Purification and aqueous phase atomic force microscopic observation of recombinant P2X2 receptor.	European Journal of Pharmacology	518	107-110	2005
Kakaoka, Ryusuke Tsuchiya, Toshie	Enhencement of Differation and Homostasis of Human Osteoblasts by Interaction with Hydroxyapatite in Form.	Key Engineering Materials	309-311	1293-1296	2006
Nagahata、Masao Kakaoka, Ryusuke Teramoto, Akira Abe, Koji Tsuchiya, Toshie	The response of normal human osteoblasts to anionic polysaccharide polyelectrolyte complexes.	Biomaterials	26	5138－5144	2005
Nakaoka, Ryusuke Ahmed, Safuddin Tsuchiya, Toshie	Hydroxy apatite microsheres enhence gap junctional intercellular communication of human osteoblats composed of connexin 43 and 45.	Wiley InterSience (www.intercience.wiley.com)	online	181-186	2005
Tamai, Masao Nakaoka, Ryusuke Tsuchiya, Toshie	Cytotoxity of Various Calcium Phosphate Ceramics.	Key Engineering Materials	309-311	263-266	2006
Tamai, Masao Nakaoka, Ryusuke Isama, Kazuo Tsuchiya, Toshie	Novel Calcium Phosohate Ceramics: The Remarkable Promoting Action on the Diffeerentation of the Normal Human Osteoblasts.	Key Engineering Materials	309-311	97-100	2006
Tamai, Masao Nakaoka, Ryusuke Tsuchiya, Toshie	In vitro study on the osteogenesis of normal human osteoblasts cultured on the discs of various kinds of calcium phosphate ceramics.	Archives of BioCeramics Research (Asian BioCeramics Symposium)	5	158-161	2005

Li, Yuping Nagira, Tsutomu Tsuchiya, Toshie	The effect of hyaluronic acid on insullin secretion in HIT-T15 cells through the enhencement of gap-junctional intercellular communications.	Biomaterials	27	1437-43	2005
Nakaoka, Ryusuke Tsuchiya, Toshie	Enhancement of Differation and Homostasis of Human Osteoblasts by Interaction with Hydroxyapatite in Form.	Key Engineering Materials.	309-311	1293-1296	2006
長幡 操、寺本 彰、阿部康次、中岡竜介、土屋利江	ラット頭蓋冠由来骨芽細胞の ALPase 活性を促進する硫酸化ヒアルロン酸の効果	繊維学会誌	61	98-102	2005
Nagahata M, Nakaoka R, Teramoto A, Abe K, Tsuchiya T	The response of normal human osteoblasts to anionic polysaccharide polyelectrolyte complexes.	Biomaterials	26	5138-44	2005
Nakaoka R, Ahmed S, Tsuchiya T	Hydroxy apatite microspheres enhance gap junctional intercellular communication of human osteoblasts composed of connexin 43 and 45.	J. Biomed. Mater. Res. A	74A	181-186	2005
Tsutomu Nagira, Susan Bijoo Matthew, Yoko Yamakoshi and Toshie Tsuchiya	Enhancement of Gap Junctional Intercellular Communication of Normal Human Dermal Fibroblasts Cultured on Polystyrene Dishes Grafted with Poly-N-isopropylacrylamide (PIPAAm).	Tissue Engineering	11	1392-97	2005
Nasreen Banu, Yasmin Banu, asamune Sakai, Tadahiko Mashino and Toshie Tsuchiya	Biogradable polymers in chodrogenesis of human articular chondrocytes	J. Artificial Organs	8	184-191	2005
Tatsuhiro Akaishi, Ken Nakazawa, Kaoru Sato, Yasuo Ohno, Yoshihisa Ito	4-Hydroxynonenal modulates the long-term potentiation induced by L-type Ca2+ channel activation in the rat dentate gyrus in vitro.	Neuroscience Letters	370	155-159	2004
Ken Nakazawa, Yasuo Ohno	Desensitization of P2X2 receptor/channel pore mutants.	European Journal of Pharmacology	495	27-33	2004

Tatsuhiro Akaishi, Ken Nakazawa, Kaoru Sato, Hiroshi Saito, Yasuo Ohno, Yoshihisa Ito	Modulation of voltage-gated Ca2+ current by 4-hydroxynonenal in dentate granule cells.	Biological Pharmacological Bulletin	27	174-179	2004
Tatsuhiro Akaishi, Ken Nakazawa, Kaoru Sato, Hiroshi Saito, Yasuo Ohno, Yoshihisa Ito	Hydrogen peroxide modulates whole cell Ca2+ currents through L-type channels in cultured rat dentate granule cells.	Neuroscience Letters	356	25-28	2004
Ken Nakazawa, Hiloe Ojima, Reiko Ishii-Nozawa, KoichiTakeuchi, Yasuo Ohno	Amino acid substitutions from an indispensable disulfide bond affect P2X2 receptor activation.	European Journal of Pharmacology	483	29-35	2004
Ken Nakazawa, Yasuo Ohno	Characterization of voltage-depenent gating of P2X2 receptor/channel	European Journal of Pharmacology	508	23 - 30	2004
Saifuddin Ahmed, Toshie Tsuchiya	Novel mechanism of tumorigenesis: Increased transforming growth factor-beta 1 suppresses the expression of connexin 43 in BALB/cJ mice after implantation of poly-L-lactic acid.	J Biomed Mater Res	70	335-340	2004
Takeshi Yagami, Yuji Haishima, Toshie Tsuchiya, Akiko Tomitaka-Yagami, Hisao Kano, Kayoko Matsunaga	Proteomic Analysis of Putative Latex Allergens.	Allergy and Immunology	135	3-11	2004
Jun Yang, Akira Ichikawa, Toshie Tsuchiya	Change of the cellular function by connexin gene transfection in a hepatoma cell line	Animal cell technology	13	293-297	2004
Eiji Okada, Yuka Komazawa, Masaki Kirihara, Hideshi Inoue, Naoki Miyato, haruhiro Okuda, Toshie Tsuchiya, Yoko Ymamakoshi	Synthesis of C60 derivatives for photoaffinity labering	Tetrahedron Letters	45	527-529	2004

Misao Nagahata, Toshie Tsuchiya et. al	A novel function of N-cadherin and Connexin43 :Marked enhancement of alkaline phosphatase activity in rat calvarial osteoblast exposed with sulfated hyaluronan	Biochem. Biophys. Res. Commun	315(3)	603-611	2004
Tsuchiya T, Sakai M, Ikeda H, Mashino T, Banu Y	Biocompatible biomaterials for the human chondrocyte differentiation estimated by RT-PCR method	Animal cell technology	13	475-479	2004
Jun Yang, Akira Ichikawa, Toshie Tsuchiya	A novel function of connexin32: marked enhancement of liver function in a hepatoma cell line	Biochem. Biophys. Res. Commun	18;307(1)	80-85	2003
Ryusuke Nakaoka, Toshie Tsuchiya, Akitada Nakamura	Neural differentiation of midbrain cells on various protein-immobilized polyethylene films	J Biomed Mater Res	64A	439-446	2003
Kazuo Isama, Toshie Tsuchiya	Enhancing effect of poly(L-lactide) on the differentiation of mouse osteoblast-like MC3T3-El cells	Biomaterials	24	3303-3309	2003
Saifuddin Ahmed, Toshie Tsuchiya	Different Expression of gap junctional protein connexin43 in two strains of mice after one-month implantation of poly-l-lactic acid.	Animal cell Technology	13	481-485	2004
Jeongung Park and Toshie Tsuchiya	Evaluation of the cornea cells affected by multi-purpose solutions for contact -lens.	Animal cell Technology	13	505-509	2004
Jun Yang, Akira Ichikawa, Toshie Tsuchiya	Change of the cellular function by connexin gane transfection in a hepatoma cell lene.	Animal cell Technology	13	293-297	2004
Taizo Sumide, Toshie Tsuchiya	Effects of Multipurpose Solutions (MPS) for Hydrogel Contact Lenses on Gap-Junctional Intercellular Communication (GJIC) in Rabbit Corneal Keratocytes	J. Biomed Mater. Res PartB:Appl Biomater	64B	57-64	2003
Kazuo Isama, Toshie Tsuchiya	Osteoblast differentiation and apatite formation on gamma-irradiated PLLA sheets.	Key Engineering Materials.	288-289	409-412	2005

Oncogene (2006) 00, 1–10

www.nature.com/onc

ORIGINAL ARTICLE

Involvement of adaptor protein Crk in malignant feature of human ovarian cancer cell line MCAS

H Linghu[1,5], M Tsuda[1,2], Y Makino[1,2], M Sakai[1,2], T Watanabe[1,2], S Ichihara[1,2], H Sawa[1,2,4], K Nagashima[1,2], N Mochizuki[3] and S Tanaka[1,2]

[1]*Laboratory of Molecular and Cellular Pathology, Hokkaido University Graduate School of Medicine, Sapporo, Hokkaido, Japan;* [2]*CREST, Japan Science and Technology Cooporation, Saitama, Japan;* [3]*National Cardiovascular Center Research Institute, Osaka, Japan and* [4]*21st Century COE Program for Zoonosis Control, Japan*

Signaling adaptor protein Crk regulates cell motility and growth through its targets Dock180 and C3G, those are the guanine-nucleotide exchange factors (GEFs) for small GTPases Rac and Rap, respectively. Recently, overexpression of Crk has been reported in various human cancers. To define the role for Crk in human cancer cells, Crk expression was targeted in the human ovarian cancer cell line MCAS through RNA interference, resulting in the establishment of three Crk knockdown cell lines. These cell lines exhibited disorganized actin fibers, reduced number of focal adhesions, and abolishment of lamellipodia formation. Decreased Rac activity was demonstrated by pull-down assay and FRET-based time-lapse microscopy, in association with suppression of both motility and invasion by phagokinetic track assay and transwell assay in these cells. Furthermore, Crk knockdown cells exhibited slow growth rates in culture and suppressed anchorage-dependent growth in soft agar. Tumor forming potential in nude mice was attenuated, and intraperitoneal dissemination was not observed when Crk knockdown cells were injected into the peritoneal cavity. These results suggest that the Crk is a key component of focal adhesion and involved in cell growth, invasion, and dissemination of human ovarian cancer cell line MCAS.

Oncogene (2006) **0**, 000–000. doi:10.1038/sj.onc.1209398

Keywords: ▮; ▮; ▮; ▮

Introduction

The regulation of cell motility is a well-organized process in which cells receive information from the surrounding environment through the extracellular matrix (ECM) (Gumbiner, 1996; Lauffenburger and Horwitz, 1996; Sheetz *et al.*, 1998). Cell surface receptor molecules for the ECM, such as integrins, transmit signals to the actin cytoskeleton through the focal adhesion complex (Brugge, 1998; O'Neill *et al.*, 2000). Tyrosine kinases, such as focal adhesion kinase (FAK) or proline-rich tyrosine kinase 2 (PYK2), are activated by the ECM and their substrates, $p130^{Cas}$ (Crk associated substrate) or paxillin, may play a role in regulation of focal adhesion (Yano *et al.*, 2000; Summy and Gallick, 2003). Downstream of focal adhesion complexes, the Rho family of small GTPases, including Rho, Rac and Cdc42, regulate the reorganization of actin fibers to form stress fibers, lamellipodia and filopodia, all of which control cell motility (Hall, 1998). Although the deregulation of focal adhesion complexes may contribute to motility and invasion of tumor cells, the precise mechanism is not well understood.

Signaling adaptor protein Crk (CT10 regulated kinase), which is mostly composed of SH2 (src homology 2) and SH3 domains, was originally isolated as an avian sarcoma virus CT10 (chicken tumor 10) encoding oncogene product (Mayer *et al.*, 1988). Since the isolation of mammalian homologues of viral Crk, such as c-Crk-I and c-Crk-II (Matsuda *et al.*, 1992b), Crk has been shown to transmit signals under various stimuli including epidermal growth factor, neurotrophic growth factor and fibroblast growth factor (Tanaka *et al.*, 1993; Feller, 2001). c-Crk-II possesses one SH2 domain at the N-terminus and two SH3 domains, wheras its alternative splicing product c-Crk-I is composed of the SH2 domain and a single SH3 domain. The SH2 domain is responsible for binding to the tyrosine phosphorylated form of 130^{Cas} and paxillin, suggesting a role for Crk in regulation of the cytoskeleton (Feller, 2001). In fact, Crk has been shown to transmit signals to small GTPases by association with its downstream effectors such as Dock180 and C3G, which

Correspondence: Dr S Tanaka, Laboratory of Molecular and Cellular Pathology, Hokkaido University School of Medicine, N 15, W 7, Kita-ku, Sapporo, Hokkaido 060-8638, Japan.
E-mail: tanaka@med.hokudai.ac.jp or sitanaka@patho2.med.hokudai.ac.jp
[5]Current address: Department of Obstetrics & Gynecology, First Affiliated Hospital of Chongqing University of Medical Sciences, Chongqing 400012, China.
Received 31 July 2005; revised 28 November 2005; accepted 28 November 2005

Gml : Ver 6.0
Template: Ver 6.1

Journal: ONC ☐ Disk used
Article : npg_onc_2004-1264 Pages: 1–10

Despatch Date: 19/1/2006
OP: Solly ED: Viji

are the guanine-nucleotide exchange factors (GEFs) for Rac and Rap, respectively (Tanaka *et al.*, 1994; Gotoh *et al.*, 1995; Hasegawa *et al.*, 1996; Kiyokawa *et al.*, 1998). The activation of Rho was also reported (Tsuda *et al.*, 2002; Iwahara *et al.*, 2003).

Dock180 and its binding molecule ELMO cooperatively regulate Rac activity and are thought to be involved in the phagocytosis of apoptotic cells (Albert *et al.*, 2000; Gumienny *et al.*, 2001; Brugnera *et al.*, 2002). C3G regulates the MAP kinase and JNK pathway by activating Rap and R-Ras, respectively, following phosphorylation on tyrosine residue 504 (Tanaka *et al.*, 1997; Tanaka and Hanafusa, 1998; Mochizuki *et al.*, 2000). Studies in C3G knockout mice suggested a role for C3G in the control of cell adhesion (Ohba *et al.*, 2001).

The contribution of c-Crk to tumorigenesis was suggested by an earlier study showing that c-Crk-I induced anchorage-independent growth of rodent fibroblasts together with tyrosine-phosphorylation of p130^{Cas} (Matsuda *et al.*, 1992b). We previously reported that Crk is overexpressed in human cancers including various carcinomas and sarcomas (Nishihara *et al.*, 2002c). In addition, there are several reports describing overexpression of c-Crk-I in malignant brain tumors and lung cancers (Miller *et al.*, 2003; Takino *et al.*, 2003). Because ovarian cancer possesses prominent metastatic potential in general and frequently exhibit intraperitoneal dissemination in patients, the human ovarian cancer cell line MCAS provides an appropriate model system to study the role of Crk in tumorigenesis (Judson *et al.*, 1999; Chen *et al.*, 2001).

In Crk knockdown MCAS cells, disorganization of actin cytoskeleton and decrease of Rac activity was observed. Cell motility and invasion were also decreased in addition to the growth suppression. Crk knockdown MCAS cells lost the ability of intraperitoneal dissemination in mice. These results suggest that Crk may be involved in malignant feature of human ovarian cancer cell line MCAS.

Results

Association of Crk and its targets in MCAS cells

Because both p130^{Cas} and paxillin are major targets of the SH2 domain of Crk, the tyrosine-phosphorylation status of these proteins was examined in MCAS cells. Immunoprecipitation analysis demonstrated that p130^{Cas} and paxillin were significantly tyrosine-phosphorylated (Figure 1a), and their association with Crk was clearly demonstrated (Figure 1b). We also analysed the association of Crk and its well-known downstream effectors, including Dock180, C3G, Sos and c-Abl, by GST pull-down assay. GST-Crk-I, GST-Crk-II and GST-Crk-SH3(N) associated with these molecules in MCAS cell lysates, whereas GST alone or GST-SH2 did not (Figure 1c).

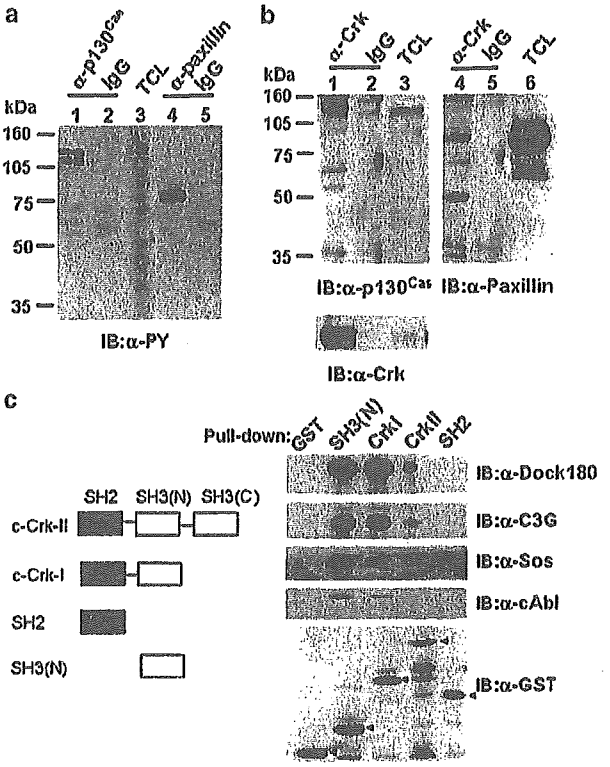

Figure 1 (a) Tyrosine phosphorylation of p130Cas and paxillin in MCAS cells. Immunoprecipitation by using anti-p130^{Cas} Ab (lane 1), antipaxillin Ab (lane 4) or control immunoglobulin (IgG, lanes 2 and 5) was performed, and probed with antiphosphotyrosine Ab. TCL, total cell lysates (lane 3). (b) Association of Crk with p130^{Cas} and paxillin. Immunoprecipitation by using anti-Crk Ab (lanes 1 and 4) or control IgG (lanes 2 and 5) was performed and probed with anti-p130^{Cas} Ab (left panel), antipaxillin Ab (right panel) or anti-Crk Ab (lower panel). (c) Association of Crk and target molecules. MCAS cell lysates were incubated with GST alone or GST fusion form of N-terminus SH3 domain of c-Crk-II (Crk-SH3(N)), c-Crk-I (CrkI), c-Crk-II (CrkII) or SH2 domain of c-Crk-II (SH2), and probed with anti-Dock180, anti-C3G, anti-Sos, anti-Abl or anti-GST Abs. Arrowheads show the calculated molecular weight of the GST fusion proteins.

Establishment of Crk knockdown MCAS cell lines and morphological analysis

To reduce expression of endogenous Crk in MCAS cells, small interfering RNA (siRNA) was employed. By using Crk siRNA in the pSUPER vector, we successfully established three independent Crk knockdown MCAS cell lines, which were designated Crki-1, Crki-2 and Crki-3. In all three cell lines, the expression of c-Crk-I was completely suppressed (Figure 2A). The expression of c-Crk-II was significantly decreased in Crki-1 and Crki-2 cells, whereas it was slightly suppressed in Crki-3 cells (Figure 2A). Endogenous protein levels of CrkL were unchanged as were those of actin (Figure 2A). The tyrosine-phosphorylation levels of p130^{Cas} and paxillin seemed to be slightly different but were statistically constant in Crk knockdown cells (Figure 2B).

In MCAS cells, filopodia and lamellipodia were readily identified at the cell edge (Figure 2C). In contrast, Crk knockdown cells tended to form small

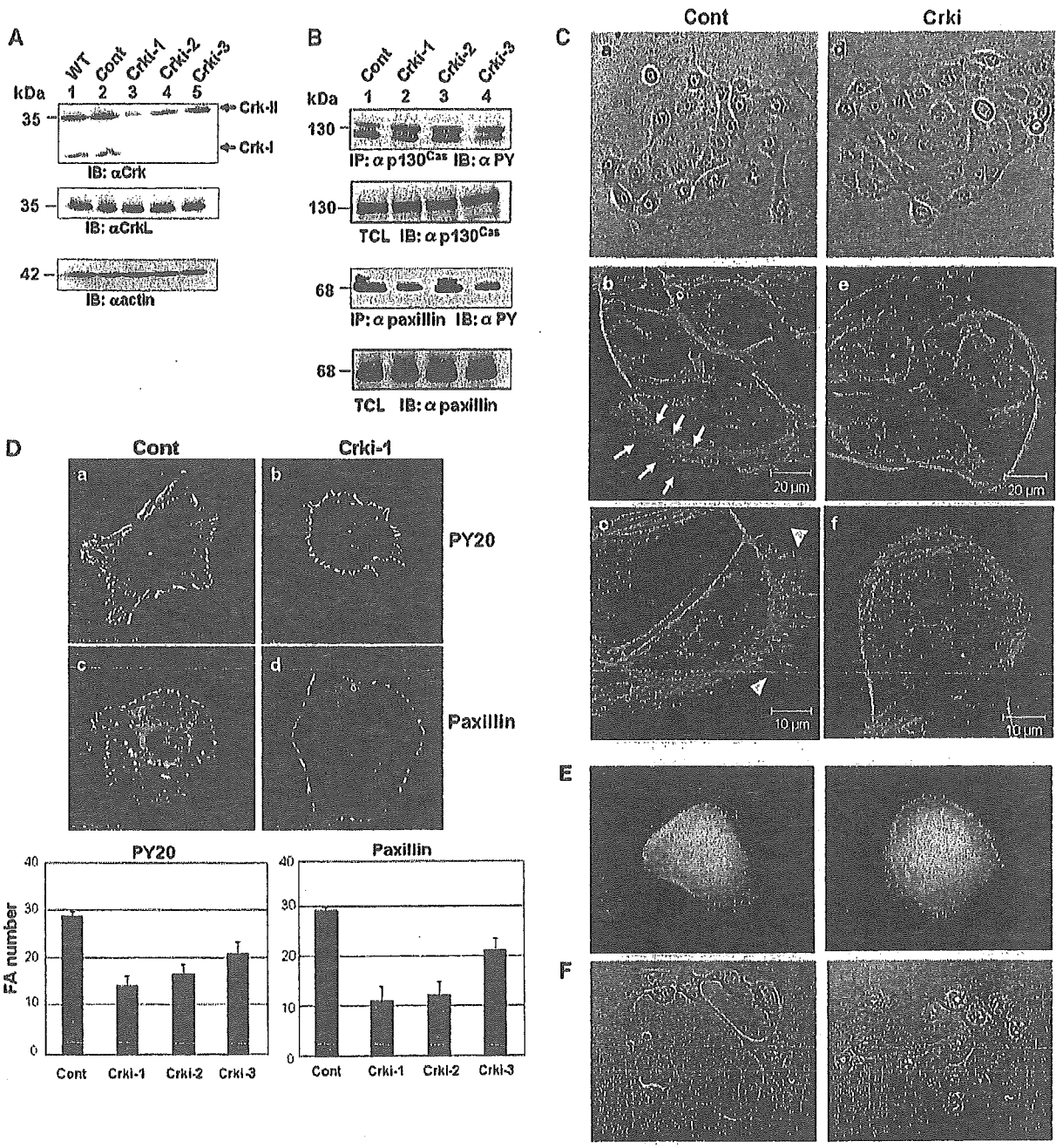

Figure 2 (A) Establishment of Crk knockdown MCAS cell lines. Total cell lysates of parental MCAS, control vector transfected cells or three Crk siRNA transfected cells (Crki-1, Crki-2 and Crki-3) were immunoblotted with anti-Crk, anti-CrkL or anti-actin Abs. The positions of Crk-I and Crk-II were indicated by arrow. (B) Tyrosine phosphorylation of $p130^{Cas}$ and paxillin in Crk knockdown cells was analysed by immunoprecipitation and immunoblotting using total cell lysate. Total levels of $p130^{Cas}$ and paxillin were also analysed by immunoblotting. (C) Morphology of parental (panels a–c) and Crk knockdown MCAS cells (panels d–f). Phase-contrast microscopical observation (panels a and d) and phalloidine staining (panels b, c, e and f). Arrow and arrowhead indicate lamellipodia and filopodia, respectively. (D) Immunofluorescence of control cells and Crk knockdown Crki-1 cells by antiphosphotyrosine (panels a and b) and antipaxillin (panels c and d) Abs. The numbers of focal adhesion were counted and described as bar graph with standard error. (E) GFP-actin transfected control (left panel) and Crk knockdown Crki-1 (right panel) cells. The results of time-lapse observation of these cells were available as Supplementary data. (F) Phase contrast microscopical observation of control (left panel) and Crk knockdown (right panel) cells 3 h after serum stimulation. (G) Transient transfection of both GFP-actin and RFP-Crk-I expression plasmids (panels a–c) or both GFP-actin and RFP (panels d–f) into Crk knockdown cells. RFP-Crk-I and GFP-actin were separately observed and displayed as upper (a and d) and middle (b and e) panels. Merged images were displayed at the bottom (c and f). The results of time-lapse observation of RFP-Crk-I expressed cells were available as Supplementary data. (H) Transient expression of myc-Crk-I and myc-Crk-II in Crk knockdown cells. Anti-myc Ab was used to detect overexpression of Crk (green). Phalloidine stain was performed to detect actin cytoskeleton (red). Yellow bar indicates 20 μm.

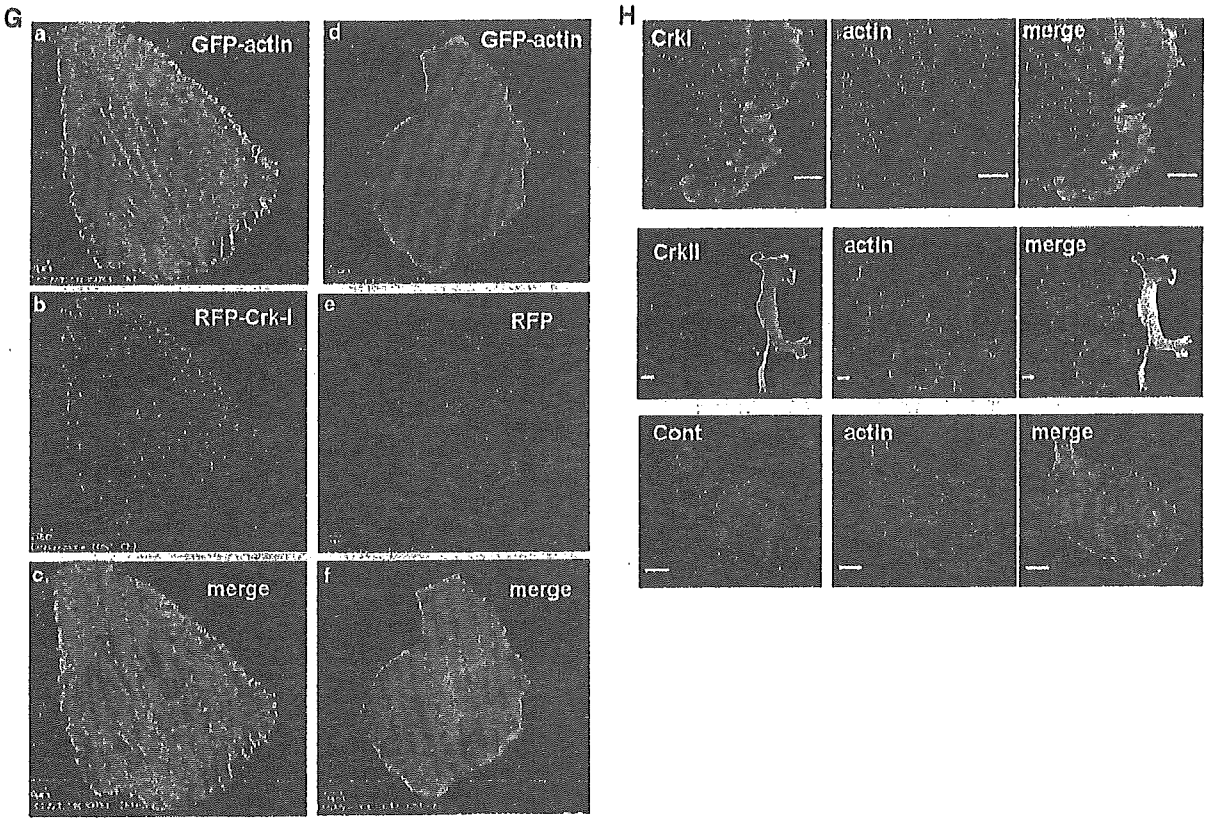

Figure 2 Continued.

clusters, and the thin cytoplasmic edge found in control MCAS cells was not observed in Crk knockdown cells in phase contrast microscopical analysis (Figure 2C). Actin staining demonstrated that dense actin bundles were present at the edge of the cytoplasm in Crk knockdown cells, and no lamellipodia was observed (Figure 2C). Immunofluorescence using antiphosphotyrosine and antipaxillin antibodies showed that the number of focal adhesions was significantly decreased in Crk knockdown cells (Figure 2D). Suppression of lamellipodia formation was confirmed by the transient transfection of the GFP fusion form of actin followed by time-lapse microscopy (Figure 2E and Supplementary data 1). Thirty-minute observations of single GFP-actin transfected cells showed that Crk knockdown cells can still move, even in the absence of lamellipodia (Figure 2E and Supplementary data 1 and 2). However, after 3 h of serum stimulation, cell scattering was much more prominent in control MCAS cells than in Crk knockdown cells (Figure 2F). To confirm the contribution of Crk to focal adhesion formation, we transiently transfected a expression plasmid for c-Crk-I fused to red fluorescent protein (RFP). Re-expression of c-Crk-I resulted in a recovery of the number of focal adhesions and also lamellipodia formation (Figure 2G and Supplementary data 3 and 4). It should be noted that in contrast to the RFP-Crk-I, we failed to transiently express RFP-Crk-II with unknown reason (data not shown). Thus, we re-expressed myc-tagged Crk-I or Crk-II in Crk knockdown MCAS cells, and found recovery of lamellipodia both by Crk-I and Crk-II (Figure 2H).

Analysis of Rac activity by pull-down assay and FRET-based time-lapse analysis

As Crk is known to regulate Rac through Dock180, we examined the activity of Rac. Consistent with the disappearance of lamellipodia, the amount of activated form of Rac was decreased in three Crk knockdown cells as determined by pull-down assay (Figure 3a). The decrease of Rac activity seemed to be correlated to the knockdown levels of Crk-II. To confirm the decrease of Rac activation, we utilized FRET-based time-lapse analysis for monitoring the activity of Rac (Itoh *et al.*, 2002). Positive signals were observed after serum stimulation in control cells, but not in Crk knockdown cells (Figure 3b and Supplementary data 5 and 6).

Analysis of motility, invasion, adhesion and matrix production of Crk knockdown cells

To clarify the effect of Crk on cell motility, a phagokinetic track assay was performed. Significantly decreased motilities of Crk knockdown cells were observed in all three Crk knockdown MCAS cells (Figure 4a). Furthermore, Crk knockdown resulted in a marked suppression of cellular invasion as was deter-

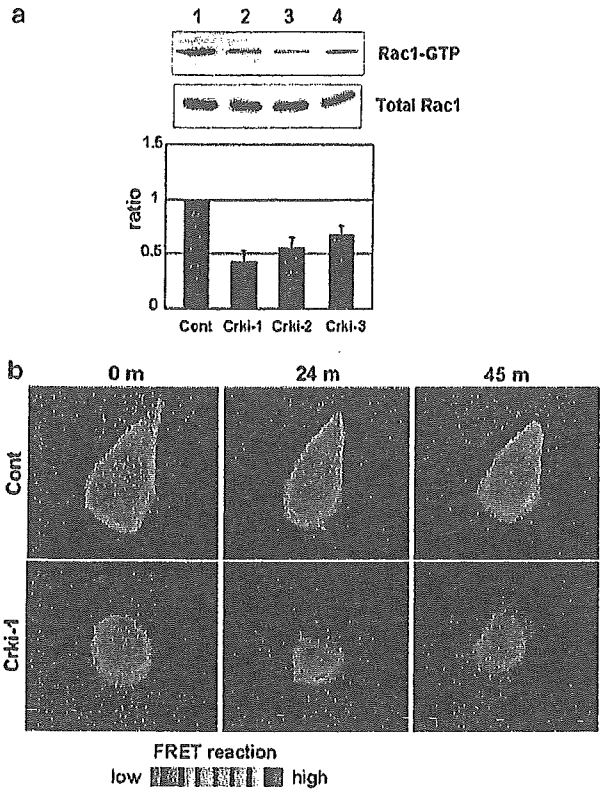

Figure 3 (a) Activity of Rac measured by pull-down assay in control and Crk knockdown cells. The GTP bound form of Rac was precipitated by GST-Pak-RBD and probed with anti-Rac Ab (upper panel). Total levels of Rac were visualized by immunoblotting using anti-Rac Ab (lower panel). Ratio of GTP-Rac and total level of Rac was quantified and described as bar graph with standard error. Lane 1, control; lane 2, Crki-1; lane 3, Crki-2; lane 4, Crki-3. (b) Time-lapse based FRET analysis of Rac activity in control (upper panels) and Crk knockdown Crki-1 (lower panels) cells 0, 24 and 45 min after 50 ng/ml of HGF stimulation. Reference of intensity was displayed at the bottom.

mined by a transwell assay (Figure 4b). As C3G was reported to regulate cell adhesion (Ohba *et al.*, 2001), an *in vitro* adhesion assay was performed. Only Crki-1 cells, not Crki-2 nor Crki-3, display a 15% reduction of adhesion on the laminin-coated culture dishes compared to control cells (Figure 4c). By pull-down assay, no significant alteration of Rap1 activity was observed in Crk knockdown MCAS cells (Figure 4d).

Anchorage-dependent and -independent growth of cells

As c-Crk has been shown to upregulate cell growth (Matsuda *et al.*, 1992a), we examined the role for Crk in growth of MCAS cells. Compared to parental cells and control cells, growth rates of three Crk knockdown cells were diminished when grown on non-coating culture plates (Figure 5a). We next examined the anchorage-independent growth of these cells by soft agar colony-forming assay. The numbers of medium sized colonies, 1.0–2.0 mm in diameter, were considerably decreased in all three of Crk knockdown cell lines (Figure 5b). Furthermore, large colonies, more than 2.0 mm in diameter, were detected in wild type and control cells, but not in Crk knockdown cells (Figure 5b). In contrast, the numbers of small sized colonies, 0.5–1.0 mm in size, were increased in Crk knockdown cells (Figure 5b).

Tumor formation assay in nude mice

Finally, we investigated the tumor-forming potential of Crk knockdown cells in nude mice. Three weeks after injection of cells, control MCAS cells formed tumors with $14 \times 10 \times 10\,mm^3$ in size and 0.8 g in weight on average. However, smaller sized tumors, with mean volumes of $10 \times 6 \times 5\,mm^3$ and mean weight of 0.4 g, were observed following injection with Crk knockdown cells (Table 1 and Figure 6a). Histopathological analysis demonstrated that control cells formed tumors with necrosis both in center and peripheral area of the tumor nodules (Table 1 and Figure 6b and c). Tumors formed by Crk knockdown cells exhibited central necrosis, but no small necrotic focus was observed in the peripheral area of the tumor (Figure 6b and c). Although the MCAS cell line was established from a surgical specimen of mucinous adenocarcinoma, the tumors formed in nude mice did not exhibit prominent mucous secretion. In contrast, in tumors formed by Crk knockdown cells, tubular formation was remarkable and significant mucous production was demonstrated by both of hematoxylin and eosin (H&E) and periodic acid Schiff (PAS) staining (Figure 6d).

We also injected established cell lines in the peritoneal cavity of nude mice and examined the potential of tumor growth as peritonitis carcinomatosa, which is one of the characteristic features of human ovarian cancer. Autopsy demonstrated that small nodules, 1.0–5.0 mm in size, were disseminated in the peritoneal cavity of mice injected with control cells (Table 1). Microscopically, tumor cells had invaded into the retroperitoneum with remarkable lymphatic vessel infiltration of the peritoneal wall (Figure 6e). In contrast, there was no evidence of tumor growth in mice injected with Crk knockdown cells (Figure 6e).

Discussion

Despite recent advancements in cancer therapy, aggressive tumors, characterized by invasion and metastasis, are still associated with poor prognosis. Among the most highly invasive human cancers, ovarian cancer, especially mucinous adenocarcinoma, is distinguishable due to its frequent intraperitoneal dissemination as well as local invasion. To control the dissemination of tumor cells, an understanding of the physiological mechanism of cell movement is important. ECM stimuli-provoked signals are transmitted, by way of cellular surface receptors such as integrins, to downstream effectors such as the Rho family of small GTPases, which play a central role in cell motility. However, regulation of the activity of small GTPases is complex and is still under investigation.

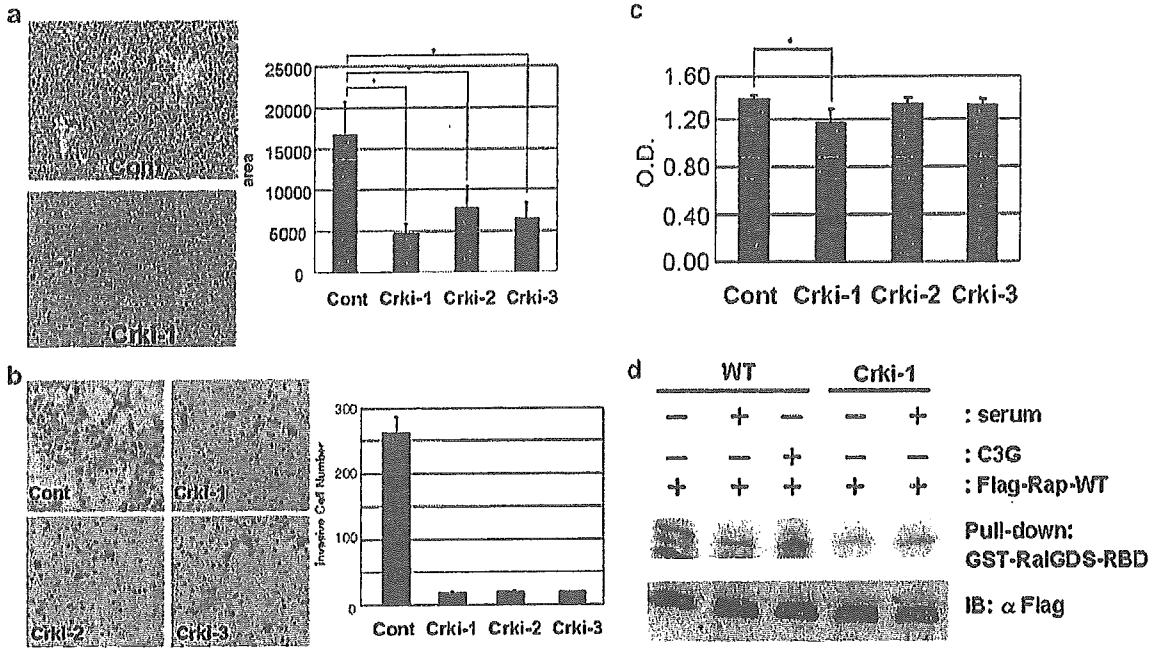

Figure 4 (a) Analysis of cell motility of control MCAS cells and Crk knockdown cells by phagocytotic track assay. Phase-contrast microscopic observation (left panels) of the moved area. Moved areas were measured and described as bar graphs (right). The difference among groups was analysed statistically by ANOVA, $F=82.9$, $P<0.01$. (b) Invasion of MCAS cells were analysed by transwell assay. The number of moved cells were counted and described as bar graph with standard error. (c) Cell adhesion was analysed on laminin-coated dishes and described as bar graph, $F=11.75$, $P<0.01$ in Crki-1 cells. No significance was found between control and Crki-2 and -3 cells. (d) Measurement of Rap activity. Wild type and Crki-1 cells were transfected with Flag-Rap1 expression plasmids and with or without serum stimulation for 30 min cells were lysed and GTP-Rap1 was precipitated by GST-RalGDS-RBD, and probed with anti-Flag tag Ab (upper panel). pCAGGAS-C3G was transfected as positive control for the assay. Total levels of exogenous Rap-1 were demonstrated by using anti-Flag tag Ab (lower panel).

Recently, we and others reported that signaling adaptor protein Crk is overexpressed in human cancers (Nishihara *et al.*, 2002c; Miller *et al.*, 2003; Takino *et al.*, 2003). Because Crk links the components of focal adhesion and GEFs for small GTPases, including Rho family proteins, overexpression of Crk may be one of the key events leading to the deterioration of cell motility. To define the precise role for Crk in malignancy of human cancers, we employed siRNA to knock down Crk expression in the human ovarian mucinous adenocarcinoma cell line MCAS. When Crk expression was diminished, cells did not form lamellipodia, probably because of the loss of focal adhesion formation as was shown by immunofluorescence study using antipaxillin and antiphosphotyrosine antibodies. Time-lapse analysis for GFP-actin transfected MCAS cells clearly confirmed that Crk knockdown decreased lamellipodia formation. In Crk knockdown cells, Rac activity was decreased and the motility and invasion potentials were also disturbed. These data suggest that Crk bound to Dock180, which is a GEF for Rac, may play a role in the regulation of motility in MCAS cells.

We did not observe compensatory overexpression of CrkL in CrkII knockdown mince (Figure 2a). By using retroviral insertional mutation technique, CrkII depleted mice were established. In these mice, the protein expression level of CrkI was intact. The authors of this paper did not examine the levels of CrkL (Imaizumi *et al.*, 1999). Furthermore, in CrkL knockout study, it is described that the expression level of CrkII was not altered in the mice lacking CrkL (Hemmeryckx *et al.*, 2002). In fact, we have established CrkII knockdown cells by using three human sarcoma cell lines and a glioblastoma cell line, and we did not observe the increase of the levels of CrkL in these cell lines (data not shown).

In general, the major components of focal adhesions have been shown to include talin, vinculin, tensin, paxillin and $p130^{Cas}$. Considering the decrease of the number of focal adhesions in Crk knockdown cells, Crk may be one of the essential components of a certain fraction of focal adhesion complexes. Because the focal adhesions still presented at the border of the cytoplasm in Crk knockdown cells, Crk may not be required to maintain the focal adhesions, at least, located at the cytoplasmic edge.

As C3G and Rap1 have been shown to regulate cell adhesion, we analysed the alteration of cell attachment to several ECMs including fibronectin, collagen, laminin and hyarulonic acid. Although, only Crki-1 cells exhibit small reduction of attachment to laminin (Figure 4c), basically, no significant suppression of attachment for ECMs was observed in Crk knockdown cells. Correlating to these results, Rap-1 activity was also not changed in Crk knockdown MCAS cells, although serum stimulation did not function as positive control for the

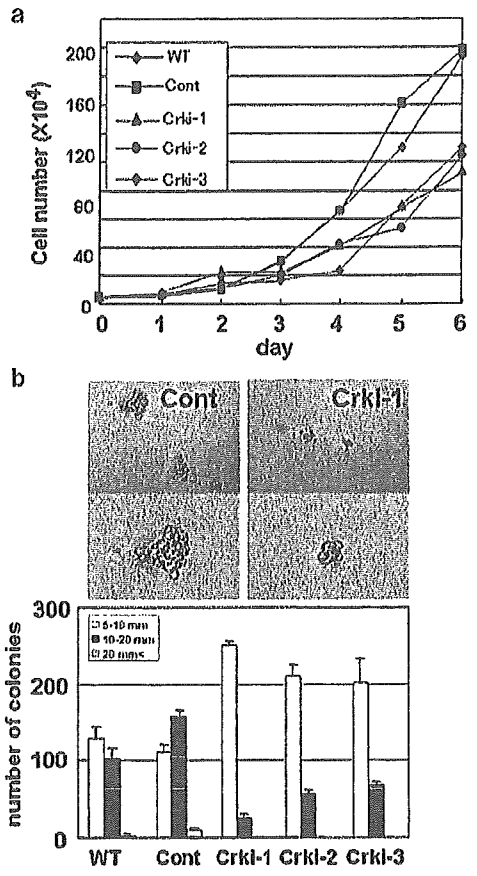

Figure 5 (a) Growth rates of control and three Crk knockdown cells were measured for 6 days on plastic plates. (b) Colony formation assay. Upper panels showed the formed colonies in soft agar. Numbers of colonies were measured and displayed as bar graph. Open bar, colonies sized 5–10 mm in diameter. Closed bar, colonies 10–20 mm in diameter and gray bar, more than 20 mm in diameter.

Table 1 Tumor formation in nude mice

	Control	*Crkl-1*	*Crkl-2*
s.c.[a] *(injected number n = 5)*			
Number	5	5	5
Size (mm)	14 × 11 × 10	10 × 6 × 5	10 × 7 × 5
Weight (g)	0.8	0.4	0.4
I.P.[b] *(injected number n = 5)*			
Number	3	0	2
Dissemination	Yes	No	No[c]

[a]s.c., subcutaneous injection. [b]i.p., intraperitoneal injection. [c]Single small nodule 2 mm in size presented.

assay (Figure 4d). Therefore, at least in MCAS cells, Crk/C3G-dependent Rap activation may not be a major mechanism of control of cell adhesion to ECMs. The reason why the effect of Crk/C3G/Rap1-dependent signaling was not dominantly observed in MCAS cells should be examined in future.

We also analysed the effect of Crk on the growth of MCAS cells, and found that growth rates of Crk knockdown cells were considerably lower than those of control cells. Thus, Crk may control the cell cycle through a C3G/R-Ras/Jun kinase-dependent mechanism, in addition to activating Ras/Erk through Sos (Tanaka *et al*., 1997; Tanaka and Hanafusa, 1998). Furthermore, the suppression of anchorage-dependent growth of Crk knockdown cells seems to be reasonable because both cell motility and proliferation were down-regulated in these cells. Subcutaneous injection of the cells into nude mice supported the *in vitro* observations suggesting that Crk may play a role in tumor cell growth and invasion. We confirmed that Crk knockdown cells did not exhibit apoptotic phenotype by using TUNEL stain and FACS analysis for cell cycle. It should be noted that Crk-I was clearly diminished in all three Crk knockdown cells, but Crk-II remained at diefferential levels. The decrease of Rac-activity in three Crk knockdown cells seemed to be related to the levels of remained Crk-II. However, there was no significant difference in the suppression of anchorage-dependent and independent growth of three Crk knockdown cells. It should be noted that we have established several Crk knockdown cells by using human sarcoma and brain tumor cell lines in which Crk-II remained differentially. But in all of the Crk knockdown cell lines, significant decrease of cell growth was observed (T Watanabe, L Wang and S Tanaka, in preparation).

Histopathological analysis showed that reduction of Crk expression enhanced the mucous production of cells. In culture, Crk knockdown cells exhibited matrix production as was demonstrated by the particle exclusion assay. Cells stained positive for PAS, implying that such matrix contains mucin, which may be indicative of cell differentiation. Together with the report that Crk has been shown to be overexpressed in tumor cells with poor prognosis (Miller *et al*., 2003), these results suggested that eliminated Crk expression may induce differentiation in tumor cells.

Intraperitoneal injection of tumor cells resulted in a remarkable difference in tumor formation between control and Crk knockdown cells. Crk knockdown cells did not form any tumors in the peritoneal cavity, while control cells produced tumor nodules with lymphoid vessel infiltration. From these results, the attenuation of cell motility, invasion or adhesion may be critical in the survival and growth of tumor cells in the peritoneal cavity. Alternatively, the production of matrix metalloproteinases (MMPs) may be involved in the tumor forming ability in the peritoneal cavity, because Crk was shown to regulate MMP production in rat fibroblasts 3Y1 cells (Liu *et al*., 2000).

The results of this study suggest that Crk may be critical for the malignant potential of MCAS cells, presumably by enhancing tumor cell motility, invasion and dissemination. Therefore, the development of a chemical compound that specifically inhibits the association of SH2 or SH3 domains of Crk to their targets may have therapeutic value in future.

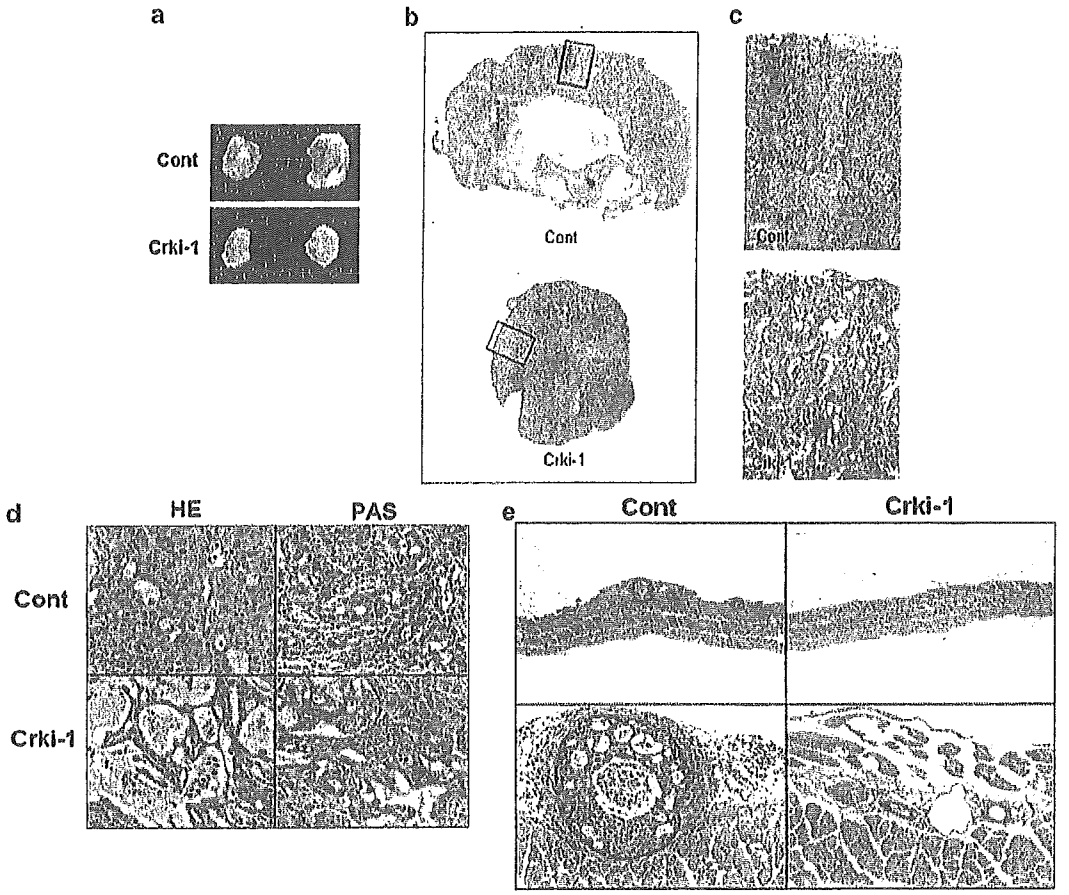

Figure 6 (a) Tumor formation of control (Cont) or Crk knockdown (Crki) MCAS cells at the back of nude mice. Macroscopic observation of surgically resected tumor nodules. (b) Histopathological analysis of resected tumors. H&E stain. (c) Histopathological analysis of peripheral region of each tumor. (d) Higher magnification of tumors. H&E and PAS stainings. (e) Analysis of the peritoneal cavity of MCAS-injected mice. Histopathological examination of peritoneal walls with H&E stain (upper panels). Lower panels showed the lymphoid vessel of the peritoneal walls.

Materials and methods

Cell lines and antibodies

MCAS, a human mucinous cystadenocarcinoma cell line (JCRB0240), was purchased from Health Science Research Resources Bank (HSRRB, Osaka, Japan) and maintained in Dulbecco's modified minimal essential medium (DMEM) supplemented with 10% fetal bovine serum (FBS), 2 mM L-glutamine, and 100 U/ml penicillin and streptomycin. The recombinant antibody (Ab) for phosphotyrosine (RC20H), mouse monoclonal antibody (mAb) for Crk (clone 22) and rabbit polyclonal Abs for $p130^{Cas}$ (C20) and paxillin, were purchased from Transduction Laboratories (Lexington, KY, USA). Antibodies for C3G (C19), CrkL (C20), and Dock180 (H4) were obtained from Santa Cruz Biotechnology (Santa Cruz, CA, USA).

Plasmids

The plasmid used for Crk interference, pSUPER (suppression of endogenous RNA)-Crk-interference (pSUPER-iCrk) with sequence of 5′-UGCCUACGACAAGACAGCC-3′ corresponding to 746–765 bp of human c-Crk-II gene, was described previously (Nagashima *et al.*, 2002). pCXN2-Flag-Crk and pCXN2-Flag-CrkL were generated in our laboratory. pGEX-Crk-I, pGEX-Crk-II, pGEX-Crk-SH3(N) and pGEX-CRK-SH3(C) were described previously (Tanaka *et al.*, 1993). pGEX-PAK2-RBD was also described previously (Nishihara *et al.*, 2002b).

Immunoprecipitation and immunoblotting

Cells were lysed with lysis buffer containing 150 mM NaCl, 10 mM Tris hydrochloride (pH 7.5), 5 mM EDTA, 10% glycerol, 0.5% Nonidet P-40, 1 mM sodium orthovanadate, 1 mM phenylmethylsulfonyl fluoride (PMSF), 50 mM sodium fluoride. Lysates were incubated with antibodies for 1 h at 4°C, followed by incubation with protein G- or protein A-sepharose beads (Calbiochem, Darmstadt, Germany) for 1 h at 4°C while rotating. Immunoprecipitates were separated by sodium dodecyl sulfate–polyacrylamide gel electrophoresis and immunoblotted onto PVDF (polyvinylidene fluoride) filter (Immobilon, Millipore Co., Bedford, MA, USA). The filter was blocked with 3% bovine serum albumin and then incubated with primary Abs followed by peroxidase-conjugated secondary Abs. Positive signals were detected by enhanced chemiluminescence system (Amersham Biosciences,

Piscataway, NJ, USA) and analysed by LAS-1000 detection system (Fuji Film, Tokyo, Japan).

Establishment of Crk knockdown MCAS cells
Cells were co-transfected with 3 μg of pSUPER-iCrk and 0.6. μg of pBabe-puro plasmid, followed by selection with 2 μg/ml puromycin containing medium for 2–3 weeks. Colonies were isolated and the expression levels of Crk were analysed by immunoblotting.

Immunofluorescence analysis of the cells
Subconfluent cells grown on glass coverslips were fixed with 3.7% formaldehyde in phosphate-buffered saline (PBS) for 15 min and permeabilized with 0.2% Triton X-100 in PBS for 5 min. To visualize actin filaments (F-actin), cells were stained with TRITC-conjugated phalloidine (1 μg/ml) for 30 min and observed under a confocal immunofluorescence microscope (Olympus, Japan). For time-lapse imaging, MCAS cells were transfected with the mammalian expression plasmid pEGFP-actin, 36 h later cells were replated onto glass dishes and GFP signal was obtained every 90 min using a time-lapse system (Nippon Roper, Chiba, Japan). Images were analysed using Metamorph software (Molecular Probe, USA).

GST pull-down assay for detection of Crk-binding proteins
Cell lysates containing 300 μg of protein were incubated with 20 μg of either GST, GST-CrkI, GST-CrkII, GST-Crk-SH2 or GST-Crk-SH3(N) for 1 h at 4°C, followed by incubation with glutathione-sepharose beads (Amersham Bioscience, Piscataway, NJ, USA) for 1 h at 4°C while rotating. Proteins bound to the beads were analysed by immunoblotting.

Pull-down assay for Rac1 activity
Detection of the GTP-bound form of Rac1 was performed as described previously (Nishihara *et al.*, 2002a). Cells were lysed with buffer containing 25 mM HEPES (pH 7.4), 150 mM NaCl, 10% glycerol, 1 mM EDTA, 1% NP40, 10 mM $MgCl_2$, 1 μg/ml aprotinin and 1 mM PMSF. Lysates were centrifuged at 12 000 r.p.m. at 4°C for 1 min, and the supernatants were incubated with 10 μg of purified GST-PAK2-RBD and glutathione-Sepharose 4B beads. The resulting precipitants were analysed by immunoblotting with anti-Rac1.

FRET-based analysis of Rac activity
pRachu-Rac-CAAX was transfected into MCAS cells, and 30 h later cells were cultured in DMEM with 2% FBS for 8 h. After 10% FBS stimulation, FRET-based analysis of Rac activity was performed following the methods established by Dr M Matsuda (Osaka University, Japan) (Itoh *et al.*, 2002).

Phagokinetic track assay
To analyse cell motility, 2×10^3 cells in DMEM were spread on 24×24 mm^2 coverslips precoated with 1% BSA and colloidal gold particles. After incubating for 24 h, cells were fixed with 3.5% formaldehyde, and the phagokinetic range for each cell was measured using Image Gauge software (Fuji Film, Tokyo, Japan).

Adhesion assay
For analysis of adhesion, 4×10^4 cells were suspended in 0.1 ml of DMEM, plated on 96-well plates, and incubated for 1 h at 37°C. The bound cells in each well were lysed, stained with 0.1% crystal violet, and quantified by spectrophotometer at OD A590 nm.

Invasion assay
The lower surface of the filter Bio Coat Matrigel Invasion Chamber (BD Biosciences, Franklin Lakes, NJ, USA) was coated with 1 μg of collagen. Fifty thousands cells were seeded in the upper chambers (24-well chambers) in 0.5 ml of serum-free medium containing 0.01% BSA and 3.3 mM glucose, and the bottom chambers contained the appropriate medium with 1% FBS as a chemo-attractant. The non-invading cells on the upper surface of the filters were removed by wiping with a cotton swab. Cells at the bottom side of the membranes were fixed with ethanol, and stained with 0.5% methyl blue. The number of cells invading through the matrigel membrane was counted in microscopic fields at $\times 200$ magnification. To minimize the bias, at least three randomly selected fields were counted. Data were averages of triplicate determinants for each condition.

Measurement of growth rates
To measure growth rates, 1×10^5 cells were seeded onto 60-mm diameter plates with DMEM containing 10% FBS, and the numbers of cells were counted everyday using a hemocytometer (Fisher Scientific).

Colony formation assay
To analyse the anchorage-independent growth of cells, 1×10^4 of cells were plated in 60-mm diameter plates with 3 ml of 0.4% noble agar in DMEM in 10% FBS, overlaying 5 ml of 0.5% bacto agar in DMEM with 10% FBS. Colonies were scored 3 weeks after plating. The number of colonies larger than 5 mm in diameter was counted under a microscope.

In vivo *tumor formation assay in nude mice*
MCAS-Crki1 cell line, in which the expression levels of both c-Crk-I and c-Crk-II was most efficiently suppressed among three established clones (Figure 2a), were injected into mice. Subcutaneously or intraperitoneally, 1×10^6 cells were injected into three of the 6-week-old female nude mice, BALB/cA Jcl-nu (nu/nu) (CLEA Japan Inc., Japan). The mice were euthanized 21–24 days after injection, and tumors were removed and weighed. A histopathological examination was performed, including hematoxylin and eosin stain and periodic acid Schiff stain.

Acknowledgements

We thank Dr Michiyuki Matsuda (Osaka University, Japan) for setting up a FRET-based time-lapse microscopy and the providing plasmids for monitoring the activity of small GTPases in a single cell. This study was supported in part by the Japan–China Sasakawa Medical Fellowship, by Grants-in-Aid from the Ministry of Education, Science, Culture, and Sports, and of the Ministry of Health, Labor, and Welfare.

References

Albert ML, Kim J-I, Birge RB. (2000). *Nat Cell Biol* **2**: 899–905.

Brugge JS. (1998). *Nat Genet* **19**: 309–311.

Brugnera E, Haney L, Grimsley C, Lu M, Walk SF, Tosello-Trampont AC *et al.* (2002). *Nat Cell Biol* **4**: 574–582.

Chen Z, Fadiel A, Feng Y, Ohtani K, Rutherford T, Naftolin F. (2001). *Cancer* **92**: 3068–3075.
Feller SM. (2001). *Oncogene* **20**: 6348–6371.
Gotoh T, Hattori S, Nakamura S, Kitayama H, Noda M, Takai Y *et al.* (1995). *Mol Cell Biol* **15**: 6746–6753.
Gumbiner BM. (1996). *Cell* **84**: 345–357.
Gumienny TL, Brugnera E, Tosello-Trampont AC, Kinchen JM, Haney LB, Nishiwaki K *et al.* (2001). *Cell* **107**: 27–41.
Hall A. (1998). *Science* **279**: 509–514.
Hasegawa H, Kiyokawa E, Tanaka S, Nagashima K, Gotoh N, Shibuya M *et al.* (1996). *Mol Cell Biol* **16**: 1770–1776.
Hemmeryckx B, Reichert A, Watanabe M, Kaartinen V, de Jong R, Pattengale PK *et al.* (2002). *Oncogene* **21**: 3225–3231.
Imaizumi T, Araki K, Miura K, Araki M, Suzuki M, Terasaki H *et al.* (1999). *Biochem Biophys Res Commun* **266**: 569–574.
Itoh RE, Kurokawa K, Ohba Y, Yoshizaki H, Mochizuki N, Matsuda M. (2002). *Mol Cell Biol* **22**: 6582–6591.
Iwahara T, Akagi T, Shishido T, Hanafusa H. (2003). *Oncogene* **22**: 5946–5957.
Judson PL, He X, Cance WG, Van Le L. (1999). *Cancer* **86**: 1551–1556.
Kiyokawa E, Hashimoto Y, Kobayashi S, Sugimura H, Kurata T, Matsuda M. (1998). *Genes Dev* **12**: 3331–3336.
Lauffenburger DA, Horwitz AF. (1996). *Cell* **84**: 359–369.
Liu E, Thant AA, Kikkawa F, Kurata H, Tanaka S, Nawa A *et al.* (2000). *Cancer Res* **60**: 2361–2364.
Matsuda M, Reichman CT, Hanafusa H. (1992a). *J Virol* **66**: 115–121.
Matsuda M, Tanaka S, Nagata S, Kojima A, Kurata T, Shibuya M. (1992b). *Mol Cell Biol* **12**: 3482–3489.
Mayer BJ, Hamaguchi M, Hanafusa H. (1988). *Nature* **332**: 272–275.
Miller CT, Chen G, Gharib TG, Wang H, Thomas DG, Misek DE *et al.* (2003). *Oncogene* **22**: 7950–7957.
Mochizuki N, Ohba Y, Kobayashi S, Otsuka N, Graybiel AM, Tanaka S *et al.* (2000). *J Biol Chem* **275**: 12667–12671.
Nagashima K, Endo A, Ogita H, Kawana A, Yamagishi A, Kitabatake A *et al.* (2002). *Mol Biol Cell* **13**: 4231–4242.
Nishihara H, Maeda M, Oda A, Tsuda M, Sawa H, Nagashima K *et al.* (2002a). *Blood* **100**: 3968–3974.
Nishihara H, Maeda M, Tsuda M, Makino Y, Sawa H, Nagashima K *et al.* (2002b). *Biochem Biophys Res Commun* **296**: 716–720.
Nishihara H, Tanaka S, Tsuda M, Oikawa S, Maeda M, Shimizu M *et al.* (2002c). *Cancer Lett* **180**: 55–61.
Ohba Y, Ikuta K, Ogura A, Matsuda J, Mochizuki N, Nagashima K *et al.* (2001). *EMBO J* **20**: 3333–3341.
O'Neill GM, Fashena SJ, Golemis EA. (2000). *Trends Cell Biol* **10**: 111–119.
Sheetz MP, Felsenfeld DP, Galbraith CG. (1998). *Trends Cell Biol* **8**: 51–54.
Summy JM, Gallick GE. (2003). *Cancer Metastasis Rev* **22**: 337–358.
Takino T, Nakada M, Miyamori H, Yamashita J, Yamada KM, Sato H. (2003). *Cancer Res* **63**: 2335–2337.
Tanaka S, Hanafusa H. (1998). *J Biol Chem* **273**: 1281–1284.
Tanaka S, Hattori S, Kurata T, Nagashima K, Fukui Y, Nakamura S *et al.* (1993). *Mol Cell Biol* **13**: 4409–4415.
Tanaka S, Morishita T, Hashimoto Y, Hattori S, Nakamura S, Shibuya M *et al.* (1994). *Proc Natl Acad Sci USA* **91**: 3443–3447.
Tanaka S, Ouchi T, Hanafusa H. (1997). *Proc Natl Acad Sci USA* **94**: 2356–2361.
Tsuda M, Tanaka S, Sawa H, Hanafusa H, Nagashima K. (2002). *Cell Growth Differ* **13**: 131–139.
Yano H, Uchida H, Iwasaki T, Mukai M, Akedo H, Nakamura K *et al.* (2000). *Proc Natl Acad Sci USA* **97**: 9076–9081.

Supplementary Information accompanies the paper on Oncogene website (http://www.nature.com/onc)

Molecular Biology of the Cell
Vol. 17, 000–000, February 2006

MAGI-1 Is Required for Rap1 Activation upon Cell–Cell Contact and for Enhancement of Vascular Endothelial Cadherin-mediated Cell Adhesion[D] [V]

Atsuko Sakurai, Shigetomo Fukuhara, Akiko Yamagishi, Keisuke Sako, Yuji Kamioka, Michitaka Masuda, Yoshikazu Nakaoka, and Naoki Mochizuki

Department of Structural Analysis, National Cardiovascular Center Research Institute, Suita, Osaka 565-8565, Japan

Submitted July 19, 2005; Revised November 28, 2005; Accepted November 29, 2005
Monitoring Editor: Martin A. Schwartz

Rap1 is a small GTPase that regulates adherens junction maturation. It remains elusive how Rap1 is activated upon cell–cell contact. We demonstrate for the first time that Rap1 is activated upon homophilic engagement of vascular endothelial cadherin (VE-cadherin) at the cell–cell contacts in living cells and that MAGI-1 is required for VE-cadherin-dependent Rap1 activation. We found that MAGI-1 localized to cell–cell contacts presumably by associating with β-catenin and that MAGI-1 bound to a guanine nucleotide exchange factor for Rap1, PDZ-GEF1. Depletion of MAGI-1 suppressed the cell–cell contact-induced Rap1 activation and the VE-cadherin-mediated cell–cell adhesion after Ca^{2+} switch. In addition, relocation of vinculin from cell–extracellular matrix contacts to cell–cell contacts after the Ca^{2+} switch was inhibited in MAGI-1-depleted cells. Furthermore, inactivation of Rap1 by overexpression of Rap1GAPII impaired the VE-cadherin-dependent cell adhesion. Collectively, MAGI-1 is important for VE-cadherin-dependent Rap1 activation upon cell–cell contact. In addition, once activated, Rap1 upon cell–cell contacts positively regulate the adherens junction formation by relocating vinculin that supports VE-cadherin-based cell adhesion.

AQ: A

INTRODUCTION

Intercellular adhesion of vascular endothelial cells is essential for connecting neighboring endothelial cells to develop a vascular tree and to function as a barrier separating blood and tissues. Vascular endothelial cell adhesion is characterized by the overlapping of adherens junctions (AJs) and tight junctions (TJs). AJs are constituted by vascular endothelial cadherin (VE-cadherin) in close cooperation with platelet and endothelial adhesion molecule-1 (PECAM-1) and nectin. VE-cadherin-mediated cell adhesion depends on extracellular Ca^{2+}, but not those mediated by PECAM-1 and nectin. TJs are made up of junctional adhesion molecule (JAM) family members, occuludin, claudin-5, and nectin (reviewed in Dejana, 2004).

VE-cadherin has an extracellular domain constituted by five cadherin domains, a transmembrane domain, and a cytoplasmic domain connected to p120 catenin and β-catenin (Iyer *et al.*, 2004). Through β-catenin, VE-cadherin is linked to α-catenin that is associated with the actin cytoskeleton, which results in the maintenance of cell–cell adhesion in conjunction with cytoskeleton (Herren *et al.*, 1998; Navarro *et al.*, 1998; Kobielak and Fuchs, 2004). Tyrosine-phosphorylated VE-cadherin in its cytoplasmic domain provides docking sites for signal-transmitting molecules (Esser *et al.*, 1998; Zanetti *et al.*, 2002; Hudry-Clergeon *et al.*, 2005). Conversely, cytoplasmic domain modified by phosphorylation or associated with signaling molecules triggers the inside-out signal that regulates the VE-cadherin-mediated cell adhesion (Nwariaku *et al.*, 2004). β-catenin binds to other signaling molecules including PI3-K and MAGUK with inverted domain structure-1 (MAGI-1) as well as α-catenin (Kotelevets *et al.*, 2005).

MAGI-1 consists of six PSD95/DiscLarge/ZO-1 (PDZ) domains, a guanylate kinase domain and two WW domains flanked by the first and second PDZ domain (Dobrosotskaya *et al.*, 1997). Because PDZ domains are docking domains for PDZ-binding molecules, MAGI-1 associates with a variety molecules such as NMDA (*N*-methyl-D-aspartate) receptors, PTEN, BAI-1, δ-catenin, mNET1, and β-catenin (Hirao *et al.*, 1998; Ide *et al.*, 1999;Mino *et al.*, 2000; Dobrosotskaya, 2001). These MAGI-1-associating molecules function at cell–cell contacts (Laura *et al.*, 2002). MAGI-1, therefore, functions as a scaffold molecule by localizing to cell–cell contacts. Recently, MAGI-1 is reported to biochemically form a complex with E-cadherin and β-catenin (Kawajiri *et al.*, 2000). How-

This article was published online ahead of print in *MBC in Press* (http://www.molbiolcell.org/cgi/doi/10.1091/mbc.E05-07-0647) on December 7, 2005.

[D] [V] The online version of this article contains supplemental material at *MBC Online* (http://www.molbiolcell.org).

Address correspondence to: Naoki Mochizuki (nmochizu@ri.ncvc.go.jp).

Abbreviations used: AJ, adherens junction; CFP, cyan fluorescent protein; ECM, extracellular matrix; EGFP, enhanced green fluorescent protein; FRET, fluorescence resonance energy transfer; GEF, guanine nucleotide exchange factor; GAP, GTPase activating protein; HAEC, human aortic endothelial cell; HUVEC, human umbilical vascular endothelial cell; JAM, junctional adhesion molecule; MAGI-1, MAGUK with inverted domain structure-1; GFP, green fluorescent protein; PBS, phosphate-buffered saline; PDZ, PSD95/DiscLarge/ZO-1; PECAM-1, platelet and endothelial cell adhesion molecule-1; siRNAs, small interfering RNAs; TJ, tight junction; VE-cadherin, vascular endothelial cadherin; VEC-Fc, recombinant VE-cadherin ectodomain-Fc chimera; YFP, yellow fluorescent protein.

<zjs;Article> • <zjss;Articles> • <zdoi;10.1091/mbc.E05-07-0647>

ever, the role of the E-cadherin/β-catenin–MAGI-1 complex in cell–cell junctional formation remains elusive.

Rap1 regulates cell–cell adhesion as well as cell–extracellular matrix (cell-ECM) adhesion (Bos, 2005). We have previously demonstrated that Epac-Rap1 signaling enhances VE-cadherin-dependent cell adhesion, thereby stabilizing vascular endothelial cell junctions (Fukuhara *et al.*, 2005). On cell–cell contact, C3G, a guanine nucleotide exchange factor (GEF) for Rap1, is involved in the signaling mediated by E-cadherin and nectin in epithelial cells (Hogan *et al.*, 2004; Fukuyama *et al.*, 2005). Rap1 cycles between GDP-bound inactive form and GTP-bound active form; Rap1-specific GEFs and GTPase activating proteins (GAPs) activate and inactivate Rap1, respectively. Rap1 GEF family consists of C3G (RAPGEF1), PDZ-GEF1 (RAPGEF2), PDZ-GEF2, CalDAG-GEF1, Epac, and Epac2 (Bos *et al.*, 2001).

We here investigate the involvement of MAGI-1–PDZ-GEF1 in the activation of Rap1 on vascular endothelial cell contact and demonstrate that MAGI-1 recruited to cell–cell junctions by associating β-catenin contributes to cell–cell contact-dependent activation of Rap1. In addition, the MAGI-1-mediated signal evoked upon cell–cell contact augments VE-cadherin-dependent endothelial cell adhesion. Thus, engagement of VE-cadherin activates Rap1 via MAGI-1, resulting in positive regulation of VE-cadherin-mediated cell adhesion.

MATERIALS AND METHODS

Plasmids and Adenovirus

pRaichu-Rap1, Rap1 activation monitoring-probe based on fluorescence resonance energy transfer (FRET), and Adeno-Raichu-Rap1, an adenovirus expressing Raichu-Rap1 were described previously (Mochizuki *et al.*, 2001). Adenoviruses encoding Rap1GAPII and LacZ were obtained from S. Hattori (The Institute of Medical Science, University of Tokyo) and M. Matsuda (Research Institute for Microbial Disease, Osaka University, Osaka, Japan), respectively. Endothelial cells were infected with adenovirus at the appropriate multiplicity of infection for more than 24 h before imaging. The coding sequences of human MAGI-1b (hereafter MAGI-1) and PDZ-GEF1 were amplified by PCR using human heart cDNA library as a template and resultant AQ: B DNAs were inserted into p3′ FLAG-CMV-10 (Sigma, St. Louis, MO) and pEGFP-C1 (Clontech, Palo Alto, CA). cDNAs encoding truncated MAGI-1 as indicated in Figures 3B and 4A were similarly inserted into pEGFP-C1. pCALwL-FLAG-C3G, a FLAG-tagged mammalian expression vector, was obtained from M. Matsuda (Research Institute for Microbial Disease, Osaka University, Osaka, Japan; Ohba *et al.*, 2001). pIRM21-PDZ5 expressed FLAG-tagged PDZ domain 5 of MAGI-1 and internal ribosomal entry site-driven dsFP593 (Nagashima *et al.*, 2002). HcRed-p120 catenin-expressed HcRed-tagged p120 catenin was described previously (Kogata *et* AQ: C *al.*, 2003).

Reagents and Antibodies

Purified human immunoglobulin (Ig) G Fc protein was purchased from ICN Biologicals (Cosa Mesa, CA). Glutathione Sepharose, protein A- and G-Sepharose were purchased from Amersham Biosciences (Piscataway, NJ). The rabbit polyclonal anti-MAGI-1b and anti-PDZ-GEF1 antibodies were developed in our laboratory by immunizing rabbits with recombinant glutathione S-transferase (GST)-tagged MAGI-1b (aa 1–140) or PDZ-GEF1 (aa 1–250) coupled with complete Freund's adjuvant, respectively. Anti-green fluorescent protein (GFP) antibody was generated in our laboratory. Other antibodies were purchased as follows: anti-Rap1 from Santa Cruz Biotechnology (Santa Cruz, CA); anti-FLAG (M2) and anti-vinculin from Sigma; anti-VE-cadherin, and anti-β-catenin from BD Bioscience (San AQ: D Jose, CA); anti-ZO-1 from Zymed (South San Francisco, CA), Alexa 488- or Alexa 546-labeled secondary antibodies from Molecular Probes (Eugene, OR); horseradish peroxidase-coupled goat anti-mouse and anti-rabbit IgG from Amersham Biosciences.

Cell Culture and Transfection

Human umbilical vein endothelial cells (HUVECs) and human arterial endothelial cells (HAECs) were purchased from Kurabo (Kurashiki, Japan). The cells were maintained in HuMedia-EG2 with a growth additive set as described previously (Nagashima *et al.*, 2002). Bovine aortic endothelial cells (BAECs), MDCK and 293T cells were maintained in DMEM (Nissui, Tokyo, Japan) supplemented with 10% fetal bovine serum and antibiotics (100 μg of streptomycin and 100 U of penicillin/ml). Endothelial cells and 293T cells were transfected by LipofectAMINE plus reagent (Invitrogen, Carlsbad, CA) and by the calcium phosphate method, respectively.

FRET Imaging and Fluorescence Imaging

HUVECs cultured on collagen-coated glass-base dishes were infected with Adeno-Raichu-Rap1 or transfected with pRaichu-Rap1. The structure of Raichu-Rap1 and the principle of FRET are illustrated as in Figure 1A. Cells were imaged on an Olympus IX-81 inverted fluorescence microscope (Lake Success, NY) as described previously (Nagashima *et al.*, 2002). Dual images for cyan fluorescent protein (CFP) and yellow fluorescent protein (YFP) were obtained through an XF1071 excitation filter, an XF2034 dichroic filter, and an XF3075 emission filter for CFP and an XF 3079 for YFP (Omega Scientific, Tarzana, CA), respectively. The ratio image of YFP/CFP were created by AQ: E MetaMorph 5.0 software (Universal Imaging, West Chester, PA) and displayed as an intensity-modulated display image as described previously (Nagashima *et al.*, 2002).

Quantitative FRET analysis at the cell–cell contacts was performed by dividing the intensity of YFP by that of CFP in the area defined by randomly selected 30 cell–cell contact sites. The detail was explained in the figure legend of Supplementary Figure 2. Cells expressing either fluorescence-tagged proteins (GFP, dsFP593, and HcRed) were time-lapse imaged similar to FRET imaging on an IX-81 microscope using appropriate filter sets for GFP and dsFP593.

Calcium Switch

HUVECs serum-starved for 10 h in medium 199 (Invitrogen) containing 1% bovine serum albumin (BSA) were transiently exposed to 4 mM EGTA for 30 min to chelate extracellular calcium and disrupt Ca^{2+}-dependent intercellular junctions (Volberg *et al.*, 1986). After washing, the cells were allowed to recover in complete cell calcium-containing culture media for the time indicated in the figure. AQ: F

Detection of GTP-bound Rap1

GTP-bound active Rap1 was detected according to Bos's method (Franke *et al.*, 1997). Briefly, cells starved in medium 199 containing 1% BSA for 10 h were subjected to a calcium switch or stimulated with 10 μg/ml VE-cadherin ectodomain-Fc (VEC-Fc) protein for the time indicated at the top of the figure. AQ: G,H The cells were lysed at 4°C in pulldown lysis buffer (20 mM Tris-HCl [pH 7.5], 100 mM NaCl, 10 mM $MgCl_2$, 1% Triton X-100, 1 mM EGTA, 1 mM dithiothreitol, 1 mM Na_3VO_4, 1× protease inhibitor cocktail). Precleared lysates were incubated with GST-Rap1 binding domain of RalGDS precoupled to glutathione-Sepharose beads. Proteins collected on the beads were subjected to SDS-PAGE followed by immunoblotting with anti-Rap1 antibody.

Immunocytochemistry and Confocal Imaging

Cells cultured on glass-bottom dishes were fixed with 2% formaldehyde in phosphate-buffered saline (PBS) for 30 min and permeabilized with 0.1% Triton X-100 for 10 min. Cells were blocked with 3% BSA for 30 min and incubated with anti-MAGI-1b, anti-VE-cadherin, anti-ZO-1, anti-vinculin, or anti-β-catenin antibody for 1 h at room temperature. Immunopositive reaction was visualized with Alexa 488- or Alexa 546-labeled secondary antibodies. Confocal images were obtained by an Olympus BX50WI microscope controlled by Fluoview.

Immunoprecipitation Assay

HUVECs were lysed with lysis buffer (100 mM NaCl, 50 mM Tris-HCl [pH 7.5], 1% Triton X-100, 2 mM Na_3VO_4, 1× protease inhibitor cocktail). Precleared cell lysates by centrifugation at 15,000 × *g* were incubated with antibodies. Immunoprecipitates collected on protein A- or G-Sepharose were subjected to SDS-PAGE and immunoblotting with antibodies as indicated in the figure. AQ: I

siRNA-mediated Protein Knockdown

Small interfering RNAs (siRNAs) targeted to human MAGI-1; 5′-GGACCCUUCUCAGAAGUUCCCUCAA-3′ and 5′-UUGAGGGAACUUCUGAGAAGGGUCC-3, corresponding to nt 843–867 of coding sequence of MAGI-1 cDNA, and that for PDZ-GEF1; 5′-GGGAGUAAUCAAACAAAGAAGACUU3′ and 5′-AAGUCUUCUUUGUUUCAUUACUCCC3′, corresponding to nt 1980–2004 of PDZ-GEF1, were obtained from Invitrogen. VE-cadherin siRNAs were purchased from Santa Cruz Biotechnology. As a control, siRNA duplex with an irrelevant sequence was used. HUVECs were transfected with 20 nM siRNA duplexes using LipofectAMINE 2000 (Invitrogen) according to the manufacturer's instructions and incubated for 48 h after replacing fresh HuMedia-EG2.

Cell Adhesion Assay

Recombinant VEC-Fc chimeric protein was prepared as described previously (Fukuhara *et al.*, 2005). Twenty-four-well tissue culture plates were coated